

Search for High Ionizing Particles in  
*pp* Collisions at the LHC's Run-1 Using the Prototype MoEDAL Detector

B. Acharya,<sup>1,\*</sup> J. Alexandre,<sup>1</sup> P. Benes,<sup>2</sup> B. Bergmann,<sup>2</sup> J. Bernabéu,<sup>3</sup> S. Bertolucci,<sup>4</sup> A. Bevan,<sup>5</sup>  
R. Bhattacharyya,<sup>4,†</sup> H. Branzas,<sup>6</sup> P. Burian,<sup>2</sup> M. Campbell,<sup>7</sup> S. Cecchini,<sup>4</sup> Y. M. Cho,<sup>8</sup> M. de Montigny,<sup>9</sup>  
A. De Roeck,<sup>7</sup> J. R. Ellis,<sup>1,10,‡</sup> M. El Sawy,<sup>7,§</sup> M. Fairbairn,<sup>1</sup> D. Felea,<sup>6</sup> M. Frank,<sup>11</sup> J. Hays,<sup>5</sup> P.  
Q. Hung,<sup>12</sup> A. M. Hirt,<sup>13</sup> J. Janecek,<sup>2</sup> M. Kalliokoski,<sup>14</sup> A. Korzenev,<sup>15</sup> D. H. Lacarrère,<sup>7</sup> C. Leroy,<sup>16</sup>  
G. Levi,<sup>17</sup> P. Li,<sup>9</sup> A. Lioni,<sup>15</sup> J. Mamuzic,<sup>3</sup> A. Maulik,<sup>4,9</sup> A. Margiotta,<sup>17</sup> N. Mauri,<sup>17</sup> N. E. Mavromatos,<sup>1</sup>  
P. Mermod,<sup>15,¶</sup> M. Mieskolainen,<sup>14</sup> L. Millward,<sup>5</sup> V. A. Mitsou,<sup>3</sup> R. Orava,<sup>14</sup> I. Ostrovskiy,<sup>18</sup> P.-P.  
Ouimet,<sup>9,\*\*</sup> J. Papavassiliou,<sup>3</sup> B. Parker,<sup>19</sup> L. Patrizii,<sup>4</sup> G. E. Păvălaș,<sup>6</sup> J. L. Pinfold,<sup>9,††</sup> L. A. Popa,<sup>6</sup>  
V. Popa,<sup>6</sup> M. Pozzato,<sup>4</sup> S. Pospisil,<sup>2</sup> A. Rajantie,<sup>20</sup> R. Ruiz de Austri,<sup>3</sup> Z. Sahnoun,<sup>4,‡‡</sup> M. Sakellariadou,<sup>1</sup>  
A. Santra,<sup>3</sup> S. Sarkar,<sup>1</sup> G. Semenoff,<sup>21</sup> A. Shaa,<sup>9</sup> G. Sirri,<sup>4</sup> K. Sliwa,<sup>22</sup> R. Soluk,<sup>9</sup> M. Spurio,<sup>17</sup> M. Staelens,<sup>9</sup>  
M. Suk,<sup>2</sup> M. Tenti,<sup>23</sup> V. Togo,<sup>4</sup> J. A. Tuszyński,<sup>9</sup> A. Upreti,<sup>18</sup> V. Vento,<sup>3</sup> O. Vives,<sup>3</sup> and A. Wall<sup>18</sup>

(THE MoEDAL COLLABORATION)

<sup>1</sup>*Theoretical Particle Physics & Cosmology Group, Physics Dept., King's College London, UK*

<sup>2</sup>*IEAP, Czech Technical University in Prague, Czech Republic*

<sup>3</sup>*IFIC, Universitat de València - CSIC, Valencia, Spain*

<sup>4</sup>*INFN, Section of Bologna, Bologna, Italy*

<sup>5</sup>*School of Physics and Astronomy, Queen Mary University of London, UK*

<sup>6</sup>*Institute of Space Science, Bucharest - Măgurele, Romania*

<sup>7</sup>*Experimental Physics Department, CERN, Geneva, Switzerland*

<sup>8</sup>*Center for Quantum Spacetime, Sogang University, Seoul, Korea*

<sup>9</sup>*Physics Department, University of Alberta, Edmonton, Alberta, Canada*

<sup>10</sup>*Theoretical Physics Department, CERN, Geneva, Switzerland*

<sup>11</sup>*Department of Physics, Concordia University, Montréal, Québec, Canada*

<sup>12</sup>*Department of Physics, University of Virginia, Charlottesville, Virginia, USA*

<sup>13</sup>*Department of Earth Sciences, Swiss Federal Institute of Technology, Zurich, Switzerland*

<sup>14</sup>*Physics Department, University of Helsinki, Helsinki, Finland*

<sup>15</sup>*Département de Physique Nucléaire et Corpusculaire, Université de Genève, Geneva, Switzerland*

<sup>16</sup>*Département de Physique, Université de Montréal, Québec, Canada*

<sup>17</sup>*INFN, Section of Bologna & Department of Physics & Astronomy, University of Bologna, Italy*

<sup>18</sup>*Department of Physics and Astronomy, University of Alabama, Tuscaloosa, Alabama, USA*

<sup>19</sup>*Institute for Research in Schools, Canterbury, UK*

<sup>20</sup>*Department of Physics, Imperial College London, UK*

<sup>21</sup>*Department of Physics, University of British Columbia, Vancouver, British Columbia, Canada*

<sup>22</sup>*Department of Physics and Astronomy, Tufts University, Medford, Massachusetts, USA*

<sup>23</sup>*INFN, CNAF, Bologna, Italy*

(Dated: June 14, 2021)

A search for highly electrically charged objects (HECOs) and magnetic monopoles is presented using  $2.2 \text{ fb}^{-1}$  of p-p collision data taken at a centre of mass energy ( $E_{CM}$ ) of 8 TeV by the MoEDAL detector during LHC's Run-1. The data were collected using MoEDAL's prototype Nuclear Track Detector array and the Trapping Detector array. The results are interpreted in terms of Drell-Yan pair production of stable HECO and monopole pairs with three spin hypotheses (0,  $1/2$  and 1). The search provides constraints on the direct production of magnetic monopoles carrying one to four Dirac magnetic charges ( $4g_D$ ) and with mass limits ranging from 590 GeV to 1 TeV. Additionally, mass limits are placed on HECO with charge in the range  $10e$  to  $180e$ , where  $e$  is the charge of an electron, for masses between 30 GeV and 1 TeV.

PACS numbers: 14.80.Hv, 13.85.Rm, 29.20.db, 29.40.Cs

The quest for intrinsically highly ionizing particle (HIP) avatars of physics beyond the Standard Model has been an active area of investigation at accelerator centres for several decades [1–15]. Searches have also been performed in cosmic rays and in matter [16, 17]. Most HIP searches can be divided into two categories: the quest for magnetic monopoles (MMs) and the hunt for highly electrically charged objects (HECOs). According to the

Bethe-Bloch formula [18], massive singly charged particles traversing matter can also be highly ionizing due to their low velocity,  $\beta$  (the particle velocity expressed as a fraction of the speed of light,  $c$ ).

In 1931 Dirac formulated a consistent description of a magnetic monopole [19] within the framework of quantum physics. This monopole is associated with a line of singularity called a Dirac string. Dirac derived his Quan-

55 tization Condition (DQC) in order that this string has no  
56 effect:

$$g = ng_D = \frac{2\pi\hbar}{\mu_0 e} n \quad (1)$$

57 where  $e$  is the electric charge of the particle probe,  $\hbar$   
58 is Planck's constant divided by  $2\pi$ ,  $g_D$  is the magnetic  
59 charge,  $\mu_0$  is the permeability of free space and  $n$  is an  
60 integer.

61 The DQC indicates that if the magnetic charge ex-  
62 ists then the electric charge is quantized in units of  
63  $e = 2\pi\hbar/(\mu_0)g_D$ . The value of  $g_D$  is approximately  $68.5e$ .  
64 Dirac's theory did not constrain the mass or the spin of  
65 the monopole. Further, the Dirac quantization condi-  
66 tion indicates a coupling strength much bigger than one:  
67  $\alpha_m = \mu_0 g_D^2 / (4\pi\hbar c) \approx 34$ . Thus, perturbation theory  
68 cannot be applied and cross-section calculations based  
69 on perturbation theory are not physically valid, although  
70 useful as a benchmark.

71 In 1974 't Hooft [20] and Polyakov [21] discovered  
72 monopole solutions of the non-Abelian Georgi-Glashow  
73 model [22]. This model has only one gauge symmetry,  
74  $SO(3)$ , with a three component Higgs field. The mass  
75 of the 't Hooft-Polyakov MM was predicted to be around  
76 100 GeV. However, MMs with such a low mass were ruled  
77 out by experiment. Subsequently, Georgi and Glashow  
78 combined their electroweak theory with a theoretical de-  
79 scription of strong nuclear forces to form a Grand Unified  
80 Theory (GUT) [23] using the single non-Abelian gauge  
81 symmetry,  $SU(5)$ . In this GUT theory the MM would  
82 have a mass of  $\sim 10^{15}$  GeV which is far too heavy to be  
83 directly produced at any foreseeable terrestrial collider.

84 Although the Standard Model has an  $SU(2) \times U(1)$   
85 group structure that does not allow a finite-energy  
86 monopole, Cho and co-workers have modified its struc-  
87 ture to admit the possibility of an "electroweak"  
88 monopole [24, 25] with a magnetic charge of  $2g_D$ . Based  
89 on this work Cho, Kim and Yoon (CKY) [26] have more  
90 recently presented an adaptation of the Standard Model -  
91 including a non-minimal coupling of its Higgs field to the  
92 square of its  $U(1)$  gauge coupling strength - that permits  
93 the possibility of a finite energy dyon [27].

94 The question of whether it is possible to create gen-  
95 eralizations of the CKY model that are consistent with  
96 the Standard Model was considered by Ellis, Mavromatos  
97 and You (EMY) [28]. EMY concluded that there is a pos-  
98 sibility that an "electroweak" monopole, consistent with  
99 the current constraints on the Standard Model, may ex-  
100 ist and be detectable at the LHC. The existence of a MM  
101 is such a theoretically well predicated and revolutionary  
102 possibility that the search for a MM has been carried out  
103 as each new energy frontier is broached.

104 We consider here only those models that admit a mag-  
105 netic charge quantized in units of Dirac charge,  $g_D$ , or a  
106 multiple of the Dirac charge. As  $g_D = 68.5e$ , a relativis-  
107 tic monopole with a single Dirac charge will ionize  $\sim 4700$

108 times more than a relativistic proton. It is thus a prime  
109 example of a HIP.

110 As mentioned above electrically charged HIPs, or  
111 HECOs, have also been hypothesized. Examples of  
112 HECOs, include: dyons, doubly charged massive parti-  
113 cles [3]; aggregates of  $ud$ - [29] or  $s$ -quark matter [30],  
114  $Q$ -balls [31], [32] and the remnants of microscopic black-  
115 holes [33].

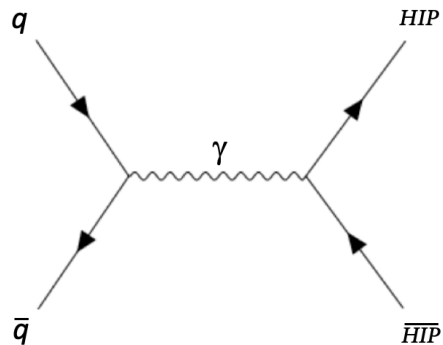


FIG. 1. Tree level Feynman diagram for DY production of HIP anti-HIP pairs.

116 The first searches for MMs and/or HECOs at the  
117 LHC were performed by the ATLAS and MoEDAL Col-  
118 laborations in 8 TeV p-p collisions [4, 5, 8]. At this  
119 stage, the ATLAS monopole search was sensitive to  
120 singly magnetically charged ( $1g_D$ ) monopoles, whereas  
121 the MoEDAL search was sensitive to single and multiply  
122 charged monopoles. ATLAS and MoEDAL continued the  
123 quest for HIPs at RUN2.

124 In the case of MMs, the ATLAS and MoEDAL searches  
125 were complementary, in the sense that ATLAS utilized  
126 the MMs highly ionizing signature [7, 14] whereas, un-  
127 til now, the MoEDAL experiment only exploited the in-  
128 duction technique to directly detect the magnetic charge  
129 [9–11]. Extensive accelerator searches for HECOs at the  
130 LHC have also been undertaken [4, 6, 7, 14]. The lat-  
131 est result from LHC describes the ATLAS experiment  
132 search for HECOs and monopoles using data taken dur-  
133 ing LHC's Run-2 at a centre-of-mass energy of 13 TeV  
134 [15].

135 In this paper we report the first use of the prototype  
136 MoEDAL Nuclear Track Detector (NTD) System, which  
137 relies on an ionization signal to detect HIPs in conjunc-  
138 tion with the prototype MoEDAL trapping detector sys-  
139 tem that utilizes a Superconducting Quantum Interfer-  
140 ence Device (SQUID) to detect the presence of trapped  
141 magnetic charge. The complete prototype detector is  
142 shown in Figure 2. A total of  $2.2 \text{ fb}^{-1}$  of  $p - p$  collision  
143 data was obtained during LHC's Run-1 at LHC intersec-  
144 tion point IP8 on the LHC ring using this detector and  
145 analyzed for evidence of HECOs.

146 A DY mechanism provides a simple model for HIP pair  
147 production. Both HECO pair production and monopole

148 pair production cross sections are computed using the  
 149 Feynman-like diagrams shown in Figure 1. It should be  
 150 noted that the large monopole-photon coupling places  
 151 such calculations in the non-perturbative regime.

## 152 THE MOEDAL DETECTOR

153 MoEDAL's detector technology is radically different  
 154 from the general-purpose LHC experiments, ATLAS  
 155 and CMS. The MoEDAL detector, deployed alongside  
 156 LHCb's VELO (VERtEX LOcator) detector at IP8, em-  
 157 ploys two unconventional passive detection methodolo-  
 158 gies tuned to the discovery of HIPs. The first of these  
 159 is a plastic Nuclear Track Detector stack array to detect  
 160 the ionization trail of HIPs. The second is a detector  
 161 system comprised of aluminium absorber elements. This  
 162 detector system is called the MMT (Magnetic Monopole  
 163 Trapper) since it was used to trap HIPs with magnetic  
 164 charge, that slow down and stop within its sensitive vol-  
 165 ume, for further laboratory analysis. Both of these de-  
 166 tector systems are passive, requiring neither a trigger or  
 167 readout electronics. The MoEDAL detector is described  
 168 in more detail below.

169 The MoEDAL detector is exemplified by its ability to  
 170 retain a permanent record, and even capture new parti-  
 171 cles for further study. The NTDs provide a tried-and-  
 172 tested and cost effective method to accurately measure  
 173 the track of a HIP and its effective charge. Importantly,  
 174 the NTD response was directly calibrated using heavy-  
 175 ion beams at the CERN SPS. The second detector sys-  
 176 tem, the MMT, ensures that a small but significant frac-  
 177 tion of the HIPs produced are slowed down, stopped and  
 178 trapped for further study in the laboratory. There are no  
 179 Standard Model particles that can produce such distinct  
 180 signatures. Thus, even the detection in MoEDAL of few  
 181 HIP messengers of new physics would herald a discovery.

### 182 Energy Loss of HIPs in MoEDAL

183 In the MoEDAL detector, HIPs loose energy by ioniza-  
 184 tion. The energy loss by ionization in the MMT detector  
 185 is computed using Bethe-Bloch formula. For NTDs, the  
 186 relevant quantity is the Restricted Energy Loss (REL)  
 187 [34]. For  $\beta < 10^{-2}$ , the REL is equal to the particle's to-  
 188 tal energy loss in the medium. At larger velocities, REL  
 189 is the fraction of the electronic energy loss leading to  
 190 the formation of  $\delta$ -rays with energies lower than a cut-off  
 191 energy  $T_{cut}$ . The REL can be computed from the Bethe-  
 192 Bloch formula restricted to energy transfers  $T < T_{cut}$  with  
 193  $T_{cut}$  a constant characteristic of the medium. For Mak-  
 194 rofrol, which is the MoEDAL NTD used for the analysis  
 195 reported in this paper,  $T_{cut} \leq 350$  eV. The RELs for  
 196 MMs and for HECOs in Makrofol are shown in Figure 3  
 197 and Figure 4, respectively.

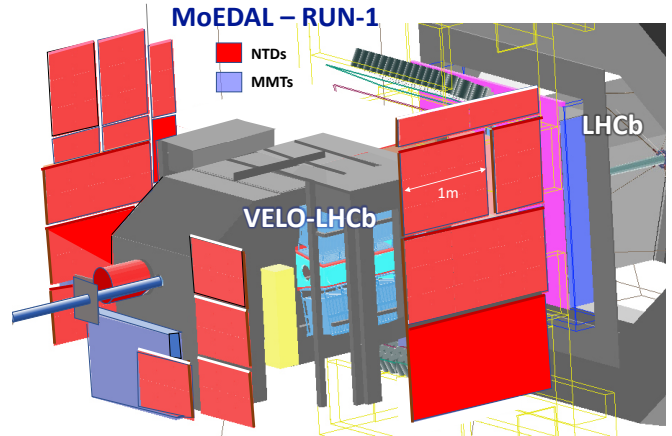


FIG. 2. A GEANT-4 Panoramix view of the MoEDAL detector prototype deployed at IP8 during LHC's RUN-1.

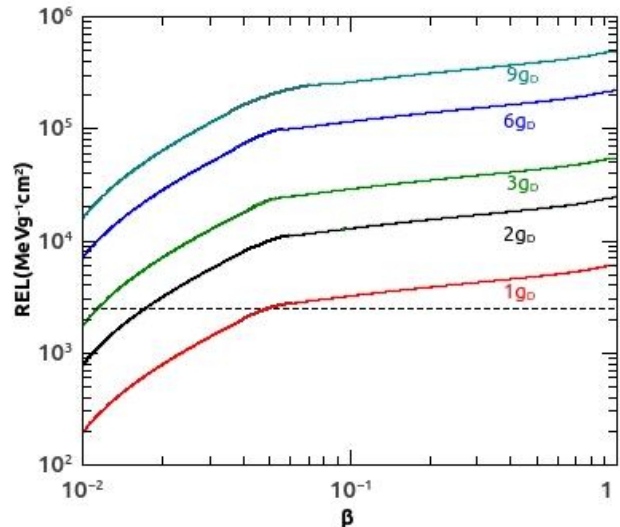


FIG. 3. Restricted Energy Loss in Makrofol for monopoles of different magnetic charge. The horizontal dotted line indicates the Makrofol detection threshold.

### The MMT Detector

199 The prototype MMT detector deployed for LHC's Run-  
 200 1 was comprised of 198 aluminium rods weighing a total  
 201 of 163 kg. These rods were housed in an enclosure placed  
 202 just underneath the beampipe at the upstream end of  
 203 LHCb's VELO detector as shown in Figure 5. After  
 204 exposure the MMT's aluminium volumes are sent to the  
 205 ETH Zurich Laboratory for Natural Magnetism where  
 206 they are passed through a SQUID magnetometer to scan  
 207 for the presence of trapped magnetic charge. A monopole  
 208 will stop in the MMT detector when its speed falls below

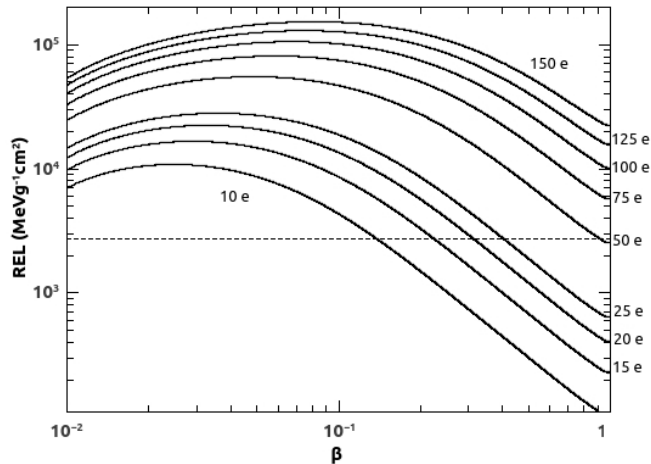


FIG. 4. Restricted Energy Loss in Makrofol for HECOs of different electric charge. The horizontal dotted line indicates the Makrofol detection threshold.

209  $\beta \leq 10^{-3}$ . It then binds due to the interaction between  
 210 the monopole and the nuclear magnetic moment [35–38]  
 211 of an aluminium nucleus comprising a MMT trapping  
 212 volume.



FIG. 5. A photograph of the prototype MMT detector deployed at IP8.

213 The anomalously large magnetic moment of an alu-  
 214 minium nucleus gives rise to a monopole-nucleus binding  
 215 energy (BE) of 0.5 - 2.5 MeV [35], comparable to the shell  
 216 model splittings. In any case, it is reasonable to assume  
 217 that the very strong magnetic field of the monopole will  
 218 rearrange the nucleus, permitting it to bind strongly to  
 219 the nucleus. As reported in Ref. [35] monopoles bound  
 220 in such a way would be trapped indefinitely. It would  
 221 require fields well in excess of several Tesla for the life-  
 222 time of the trapped monopole state to compromise its  
 223 detection by the MoEDAL trapping detector. We note

224 that the MOEDAL detector is only subject to fields lower  
 225 than  $\sim 10$  mT.

### 226 Calibration of the MMT Detector

227 A magnetic monopole captured in an MMT volume  
 228 is tagged and measured as a persistent current in the  
 229 SQUID coil encircling the samples' transport axis that  
 230 passes through the SQUID magnetometer. The calibra-  
 231 tion of the magnetometer response is achieved using two  
 232 independent techniques. In brief, the magnetometer cal-  
 233 ibration was obtained using a convolution method ap-  
 234 plied to a dipole sample, and validated using long thin  
 235 solenoids that simulate a monopole of well-known mag-  
 236 netic charge. For more details please see Ref. [39]. These  
 237 calibration methods agree to within 10%, which is taken  
 238 as the pole strength calibration uncertainty. The magne-  
 239 tometer response has been determined by measurement  
 240 to be charge-symmetric and linear in a range of magnetic  
 241 charge 0.3 - 300  $g_D$ .

### 242 The Nuclear Track Detector System

243 The MoEDAL Nuclear Track Detector is arranged in  
 244 modules deployed around IP8 in the VELO cavern. A  
 245 prototype NTD array of 125 stacks was installed for  
 246 Run-1 as shown in Figure 2. Each module comprises  
 247 three layers of 1.5 mm thick CR39<sup>®</sup> polymer, three lay-  
 248 ers of Makrofol DE<sup>®</sup> and three layers of Lexan<sup>®</sup> 0.5 and  
 249 0.25 mm thick, respectively, inside Aluminium bags (Fig-  
 250 ure 6). Currently the Lexan<sup>®</sup> foils serve as protective  
 251 layers and are not analyzed.

252 In this analysis only the Makrofol NTDs are utilized.  
 253 This is due roughly a factor ten higher detection thresh-  
 254 old in Makrofol than CR39 which results in substantially  
 255 less “visual noise” in the etched plastic large due due  
 256 to spallation products arising from beam backgrounds.  
 257 Thus, the analysis of the CR39 NTDs is considerably  
 258 more time intensive. DY produced in LHC collisions dur-  
 259 ing Run-1, are sufficiently highly ionizing that they can  
 260 easily be detected with the Makrofol NTDs obviating the  
 261 need to scan the CR39. Of course, in the event of the  
 262 observation of a candidate event in the Makrofol all 6  
 263 NTD sheets in the stack would be analyzed.

### 264 The etching procedure

265 In plastic track-etch detectors, the passage of a heav-  
 266 ily ionizing particle can produce a permanent damage of  
 267 polymeric bonds in a cylindrical region (“latent track”)  
 268 extending few tens of nanometers around the particle tra-  
 269 jectory (Figure 7). By subsequent chemical etching the  
 270 latent track is “amplified” and can be made visible under

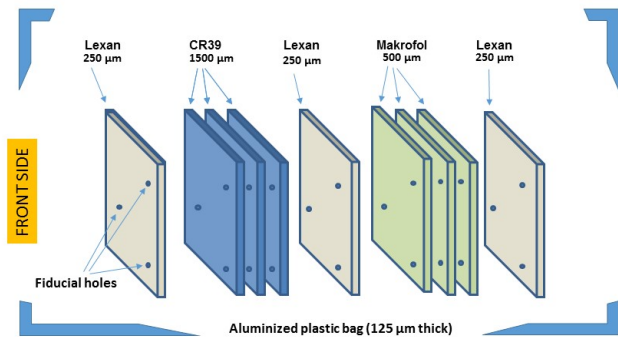


FIG. 6. NTD module composition

an optical microscope. In the etching process, the bulk of the material is removed at a rate  $v_B$  and at a higher rate  $v_T$  along the latent track. The damage zone is revealed under an optical microscope as a cone shaped etch-pit, called “track”. Etch-pits surface openings have a circular shape for normally incident particles, otherwise they are elliptical.

A sketch of an etch-pit at different etching times is shown in Figure 7 for a normally incident particle crossing the detector with a constant energy loss. Two etching conditions were applied (Table I). The first was the so-called “strong” etching [40] condition, allowing faster etching and yielding larger etch-pits that were easier to detect under visual scanning. Strong etching was applied to the first, most upstream, Makrofol foil in each module. The second, “soft etching”, condition results in a slower etching process. This allows the etching process to proceed in several steps in order to follow the formation of etch-pits. Soft etching is applied to subsequent Makrofol foils in the stack, if a candidate track is found in the first layer. In Figure 8 are shown microphotographs of relativistic  $\text{Pb}^{82+}$  tracks in Makrofol foils etched in (left) “soft conditions”; (right) “strong conditions”.

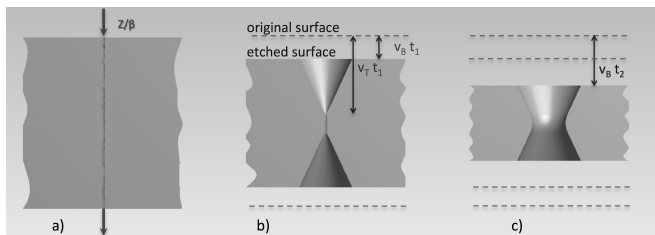


FIG. 7. Illustration of the track-etch technique: a) latent track forming along the trajectory of a high ionizing particle impinging perpendicularly on the NTD surface ; b) development of conical pits during the etching process; c) etch-pits joining after a prolonged etching, forming a hole in the detector.

294

The response of the NTD is measured by the etching rate ratio  $p = v_T/v_B$ , as a function of the particle’s REL. Heavy ion beams are used to determine the detector response over a large range of energy losses, as discussed in ref. [41]. The Makrofol was calibrated with 158 A GeV  $\text{Pb}^{82+}$  and 13 A GeV  $\text{Xe}^{54+}$  ion beams at the CERN SPS. The calibration set-up included a stack of Makrofol foils placed upstream and downstream of an Aluminum target. Incoming ions undergo charge changing nuclear fragmentation interaction along their path through the detector foils and the target. After exposure the detectors were etched in 6N KOH+20% ethyl alcohol at 50 ° C for 10 hours. The bulk etch velocity was  $v_B = 3.4 \mu\text{m/h}$ .

After etching, the size of surface tracks was measured with an automatic scanning system providing the cone base area, and the coordinates of the center of the etch pits. Etch pits diameters typically range from 10  $\mu\text{m}$  to 100  $\mu\text{m}$ , with a modal value in the range 30  $\mu\text{m}$  to 40  $\mu\text{m}$ . The base area distributions of incoming ions and of their fragments is shown in Fig. 9. The projectile fragments have the same velocity and approximately the same direction as the incident ions. From the base area spectrum, the charge corresponding to each nuclear fragment peak can be identified, and the corresponding REL determined. A detailed description of the calibration procedure can be found in [41].

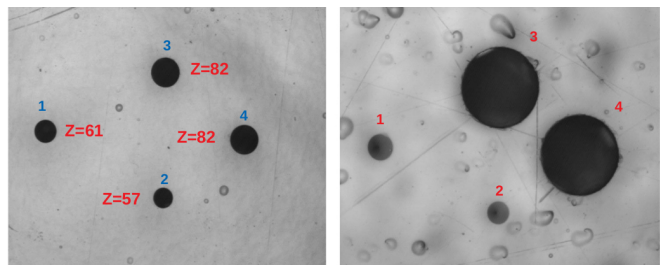


FIG. 8. Microphotographs of relativistic  $\text{Pb}^{82+}$  tracks and of nuclear fragments ( $Z < 82$ ) in two consecutive foils of Makrofol. Each image frame measures 0.64 mm x 0.80 mm. Etch pits are from the same ions crossing the detector foils: (left) Makrofol foil etched in “soft conditions”; (right) Makrofol foil etched in “strong conditions”. Note that the microphotographs also show two clearly differentiated fragmentation products of Pb: La ( $Z = 57$ ); and, Pm ( $Z=61$ ).

For each identified peak the reduced etch rate  $p$ , the  $Z/\beta$  and eventually the restricted energy loss are computed (Fig.9). Calibration data thus obtained are shown in Fig.10. The minimum detectable relativistic charge is  $Z/\beta \geq 50$ , both in soft or strong etching. The detector threshold is at REL  $\sim 2700 \text{ MeV g}^{-1}\text{cm}^2$ .

NTDs are detection threshold devices. In CR39 and in

TABLE I. Etching Conditions of Makrofol

Etching Conditions		
Etching Mode	Etchant	$v_B$ ( $\mu\text{m}/\text{hour}$ )
Strong	6N KOH + 20% ethyl alcohol at 65°C	$23 \pm 0.5$
Soft	6N KOH + 20% ethyl alcohol at 50°C	$3.4 \pm 0.05$

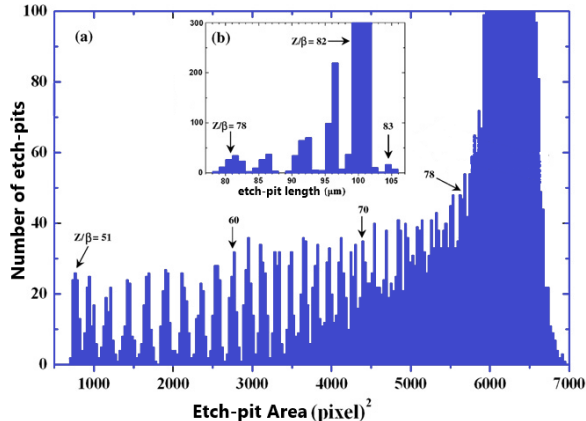


FIG. 9. Distribution of track surface areas in Makrofol exposed to 158 A GeV Pb<sup>82+</sup> and etched in soft conditions [41].

328 Makrofol the minimum REL leading to a pit formation  
 329 are 25 MeV cm<sup>-2</sup>g<sup>-1</sup> and 2500 MeV cm<sup>-2</sup>g<sup>-1</sup>, respec-  
 330 tively.

### 331 *Etching and Scanning of MoEDAL NTD*

332 After exposure in the LHC IP8 region, the MoEDAL  
 333 NTD stacks were brought to the INFN etching and scan-  
 334 ning Lab in Bologna. A global module reference system  
 335 is created by drilling three reference holes – 2 mm diam-  
 336 eter – on each detector module. This coordinate system  
 337 provides an accuracy of 100  $\mu\text{m}$  on the determination  
 338 of the position of a particle track over the detector sur-  
 339 face. The stacks are then unpacked, the detectors foils  
 340 labelled and their thickness measured on a grid of points  
 341 uniformly distributed over the foil surface.

342 For the search reported in this paper only Makrofol  
 343 foils were analysed. In each exposed stack, the most up-  
 344 stream Makrofol layer was etched in 6 N KOH + 20%  
 345 ethyl alcohol at 65°C. After 6 hours etching, etch-pits as  
 346 small as 10  $\mu\text{m}$  would be detected under 20  $\times$  magnifica-  
 347 tion. An efficiency of  $\sim 99\%$  was estimated by scanning  
 348 foils exposed to ions.

349 Each Makrofol layer examined was manually scanned.  
 350 Every detected surface structure was further observed  
 351 under higher magnification and classified either as ma-  
 352 terial defects or particle’s track. If a pair of etch-pits is  
 353 detected on the front and back sides of the foil, it was  
 354 observed at larger (100 - 500 $\times$ ) magnification. From the

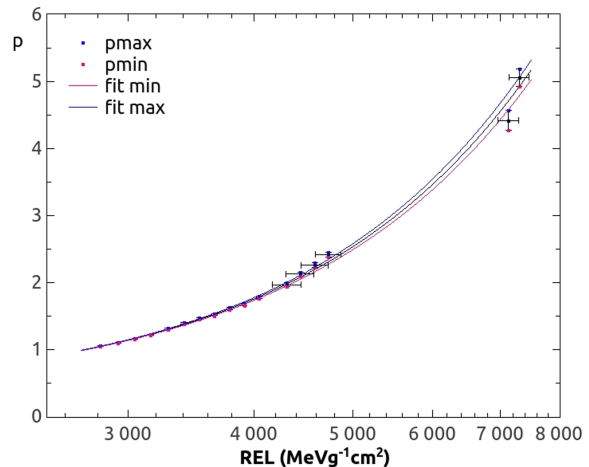
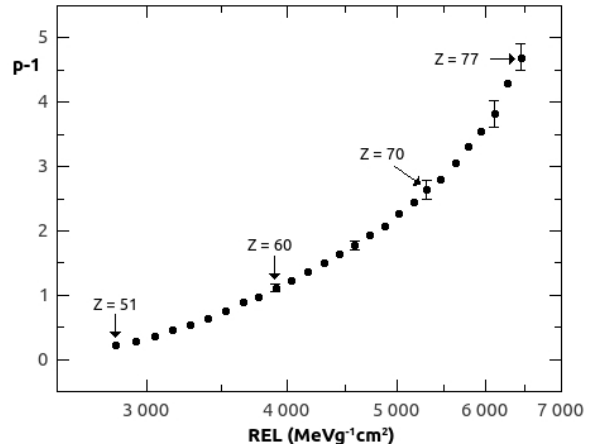


FIG. 10. Reduced etch-rate versus REL for Makrofol exposed to relativistic Lead and Xenon ion beams: (top) detectors etched in soft conditions;(bottom) detectors etched in strong conditions. The upper and low curves are drawn through the  $\pm 1\sigma$  value of the error on each  $p$  value, where the error bars represent a convolution of the statistical and systematic error on each point.

355 etch-pit size on the “front” and “back” surfaces, and the  
 356 bulk etching rate, the incidence angle on each surface is  
 357 estimated. It takes around 2.5 hours to scan one side of  
 358 a Makrofol layer when using the Jenatec microscope at  
 359 32 $\times$  total magnification.

360 A track was defined as a potential “candidate” if etch-  
 361 pit sizes as well as incidence and exit angles on the front

362 and back surfaces. Such a candidate would be checked  
 363 further by looking for collinear etch pits in the down-  
 364 stream NTD in the same stack. Additionally, the track  
 365 formed by all the collinear etch pits would need to be  
 366 compatible with pointing towards the interaction point,  
 367 IP8, before it can be claimed to be a true candidate for  
 368 a HIP avatar of new physics. The vast majority of spal-  
 369 lation products arising from beam backgrounds have a  
 370 very limited range in the NTD sheet, typically tens of  
 371 microns, and only give rise to a single pit when the NTD  
 372 sheet is etched. If candidates were found in the first layer  
 373 of a module, downstream Makrofol foils would be etched  
 374 in 6 N KOH + 20% ethyl alcohol at 50°C and etch-pits'  
 375 dimensions (surface area, etch-pit length) measured in  
 376 order to determine the particle's direction and REL.

377 An accurate scan under an optical microscope with  
 378 high magnification (100 - 200  $\times$ ) is performed in a square  
 379 region of about 1 cm<sup>2</sup> around the candidate expected  
 380 position. If a two-fold coincidence was detected, also the  
 381 middle layer would be etched and analyzed. However, no  
 382 candidate was found.

383 If no candidates were found in the first Makrofol foil  
 384 in a stack, no other foils would be scanned. However,  
 385 the CR39 foils all stacks are retained for future analyses,  
 386 where the the REL threshold is much lower, roughly ten  
 387 times less than Makrofol.

#### 388 *The Detection Threshold for Makrofol*

389 For the HIP to be detected its REL must be greater  
 390 than the detection threshold of the Makrofol. The detec-  
 391 tion threshold will vary with the etching conditions. It  
 392 will also vary with the angle of incidence of the HIP ( $\delta$ )  
 393 on the NTD. The connection between the threshold and  
 394 the maximum angle of incidence ( $\delta_{Max}$ ) to the normal to  
 395 the NTD that the HIP can make and still be detected,  
 396 is expressed by the relationship:  $p = \frac{1}{\cos(\delta_{Max})}$ . Every-  
 397 thing else being equal, the greater the maximum angle of  
 398 incidence the lower the detection threshold. The lowest  
 399 threshold is obtained for a HIP impinging normally to  
 400 the NTD. The curve showing the relation between  $\delta_{Max}$   
 401 and the REL is shown in Figure 11.

#### 402 *Efficiency and False Positives in the NTD Detectors*

403 As described above the signal for the passage of a HIP  
 404 messenger of new physics passing through a MoEDAL  
 405 NTD stack would be a string of etch pits in the stack,  
 406 where an etch pit pair is due to the ingress and egress of  
 407 the HIP passing through an NTD sheet. No such signal  
 408 has ever been seen in this search, or by any other HIP  
 409 search employing NTDs [2]. Indeed, no candidates, or  
 410 false positives as they would be classified as candidate,

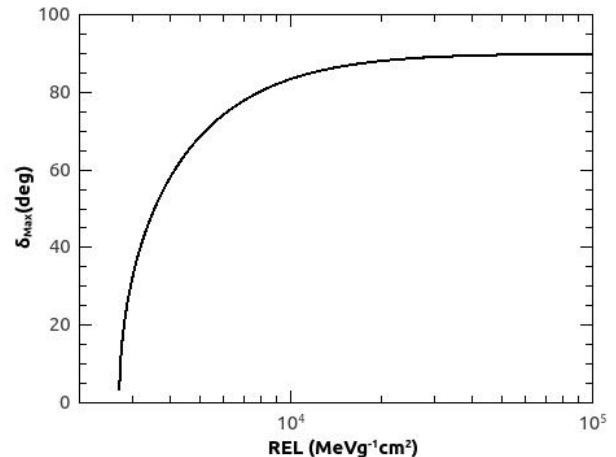


FIG. 11. The maximum angle to the normal of the NTD plane within which the HIP will be detected.

411 were seen in the 125 stacks examined (corresponding to  
 412 7.8 m<sup>2</sup>), where only the most upstream sheet of the NTD  
 413 stacks were examined.

414 The absence of false positives using the NTD tech-  
 415 nique is borne out by the astroparticle physics exper-  
 416 iments MACRO [46] and SLIM [47], which deployed a  
 417 surface area of 1263 m<sup>2</sup> and 427 m<sup>2</sup>, respectively, and did  
 418 not observe a single HIP candidate. It should be noted  
 419 that the NTD technique employed by these experiments  
 420 are essentially identical to those employed at colliders.

421 The lack of false positives in the NTD technique at  
 422 colliders or in astroparticle physics experiment raises the  
 423 question of the false negatives, or detector efficiency. This  
 424 can be evaluated using the heavy ion beams that are  
 425 used to calibrate NTD detectors. In the absence of beam  
 426 backgrounds, the detection, or scanning, efficiency for  
 427 the etch pits due to heavy-ion HIPs with ionizing power  
 428 above the NTD threshold was measured to be in excess  
 429 of 99%.

430 In order to estimate the effect of beam background  
 431 on the detection efficiency of NTDs for HIPs we utilized  
 432 NTD calibration stacks exposed to a relativistic lead-ion  
 433 beam as described above. The stacks were comprised  
 434 of sheets of Makrofol NTDs exposed to the beam back-  
 435 grounds in the VELO cavern at the LHC for a year of  
 436 data taking interleaved with unexposed Makrofol NTD  
 437 sheets. Plastic from the same production batch was used  
 438 in calibration and standard data taking.

439 The NTDs sheets comprising the calibration stacks  
 440 were then etched in the same way as the standard NTD  
 441 stacks deployed for data taking during Run-1. The in-  
 442 dividual sheets were then scanned using the same man-  
 443 ually controlled optical scanning microscope technology  
 444 employed to examine all MoEDAL NTD stacks. The  
 445 relativistic lead-ion calibration beam particles penetrate

446 the whole stack allowing the signal etch pits seen in the  
 447 plastic sheet that was not previously exposed to the LHC  
 448 beam - where the signal can clearly be observed with a  
 449 100% efficiency - to serve as a map. This map can be used  
 450 to assess the efficiency of the scan of the adjacent NTD  
 451 sheet that had been exposed to LHC beam backgrounds.  
 452 These studies, indicate that the efficiency for detection  
 453 above threshold was in excess of 99%. This number was  
 454 determined by multiple scanning of the same sheets by  
 455 different scanners.

## 456 ACCEPTANCE OF THE RUN-1 MOEDAL 457 DETECTOR

458 The MoEDAL detector's acceptance is defined to be  
 459 the fraction of the number of events in which at least one  
 460 HIP of the Drell-Yan (DY) produced pair was detected in  
 461 MoEDAL in either the NTD detector or the MMT detector.  
 462 The acceptance for DY production of HECOs and  
 463 magnetic monopoles is described by an interplay of the  
 464 geometrical disposition of MoEDAL NTD modules and  
 465 MMT detectors, energy loss in the detectors, mass of the  
 466 particle and the spin-dependent kinematics of the inter-  
 467 action products. In the case of the HECOs, MoEDAL's  
 468 NTD system provides the only means of detection.

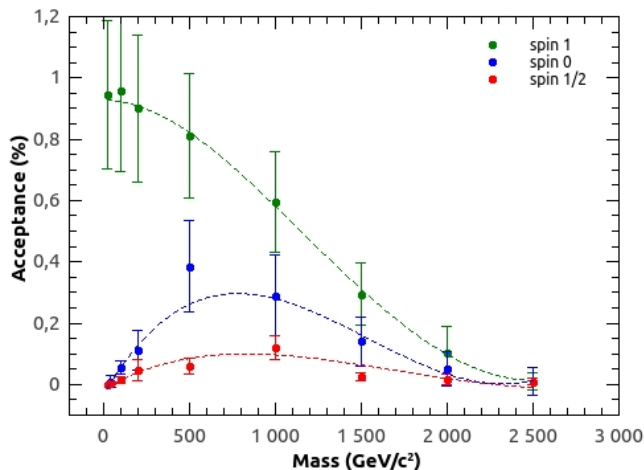


FIG. 12. Acceptance for spin-1, spin-0 and spin-1/2 HECOs with charge 125e.

469 For a given HIP mass and charge, the pair-production  
 470 model determines the kinematics and the overall trapping  
 471 acceptance obtained. The uncertainty in the accep-  
 472 tance is dominated by uncertainties in the material de-  
 473 scription [8–10]. This contribution is estimated by per-  
 474 forming simulations with hypothetical material conserva-  
 475 tively added and removed from the nominal geometry  
 476 model. An example, showing the MoEDAL NTD ac-

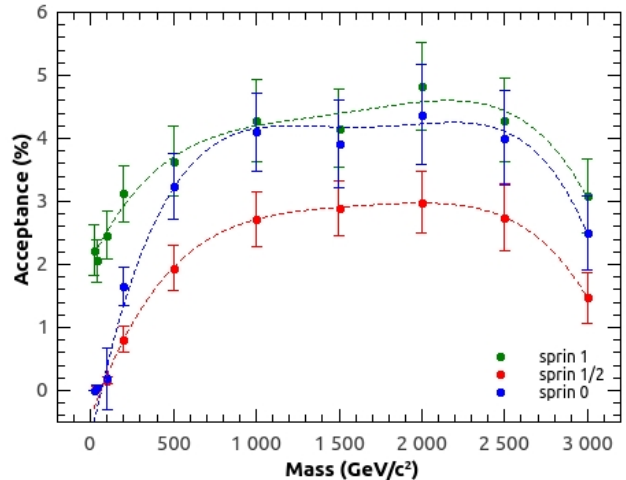


FIG. 13. Acceptance for monopole pair production with mag-  
 netic charge  $2g_D$ .

477 ceptance curves for spin-1/2, spin-0, spin-1 HECOs with  
 478 charge 125e is shown in Figure 12. The acceptance curves  
 479 for spin-0, spin-1/2 and spin-1 monopoles, found using  
 480 the NTD and MMT detectors combined, are shown in  
 481 Figure 13. The corresponding curves for spin-0 and spin-  
 482 1 monopoles follow the same general form. The accep-  
 483 tance for  $1g_D$  rises roughly quadratically to a maximum  
 484 around 2.5 TeV of nearly 11% to 12% for both spin-0 and  
 485 spin-1 monopoles. For  $2g_D$ , the acceptance curves reach  
 486 a plateau between  $\sim 500$  GeV and 2.5 TeV, of approxi-  
 487 mately 4%. The curves for  $3g_D$  follow the same form as  
 488 does that of  $2g_D$ , but the plateau is only  $\sim 2\%$ . For 4  
 489 and  $5g_D$  the acceptance reaches a very broad maximum  
 490 at less than 1% before falling to zero at 3 TeV. The ac-  
 491 ceptances shown in Figure 12 and Figure 13 refer to the  
 492 prototype detector deployed for LHC's Run-1.

## 493 ANALYSIS RESULTS

494 The first Makrofol sheet of each of MoEDAL's 125  
 495 NTD stacks, exposed during LHC's Run-1 were etched  
 496 and scanned, as described above, for evidence of the pas-  
 497 sage through the sheet of a highly ionizing object such  
 498 as a HECO or a magnetic monopole. The total area of  
 499 plastic analyzed was  $7.8 \text{ m}^2$  (Run-1). No candidate  
 500 events were observed. In addition, no monopole candi-  
 501 dates were observed to be trapped in the MMT detector.  
 502 This is the first time that the data from the MoEDAL  
 503 prototype detector, deployed during Run-1, has been pre-  
 504 sented.

505 There are two dominant sources of systematic error in  
 506 this analysis. The first arises from the imperfect knowl-  
 507 edge of the amount of material between the interaction

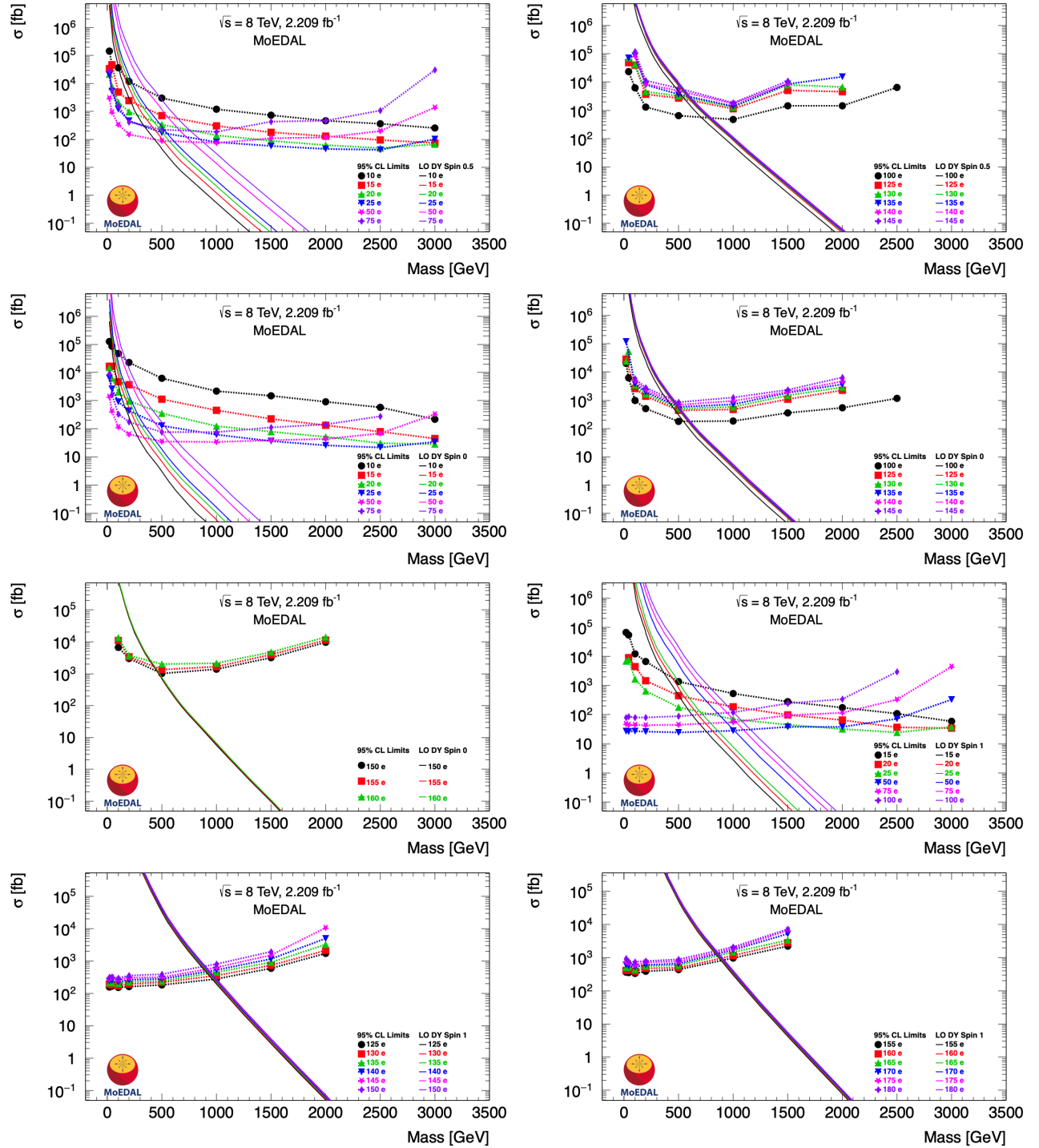


FIG. 14. 95% CL mass limits in a DY production model of spin-0, spin-1/2 and spin-1 HECO pair direct production in LHC  $pp$  collisions.

508 point and the MoEDAL NTD modules, due to LHCb's  
 509 VELO detector. The VELO vacuum vessel and the various  
 510 elements of the VELO detector with LHCb's acceptance  
 511 are simulated with great precision in the LHCb  
 512 geometry. However, detailed technical drawings of other

513 elements of VELO upstream of the sensitive elements of  
 514 VELO such as cables, in-situ electronics, cooling pipes,  
 515 various flanges, a vacuum pump and a vacuum manifold,  
 516 are not available.

517 Nominally, this intervening material is between 0.1 and

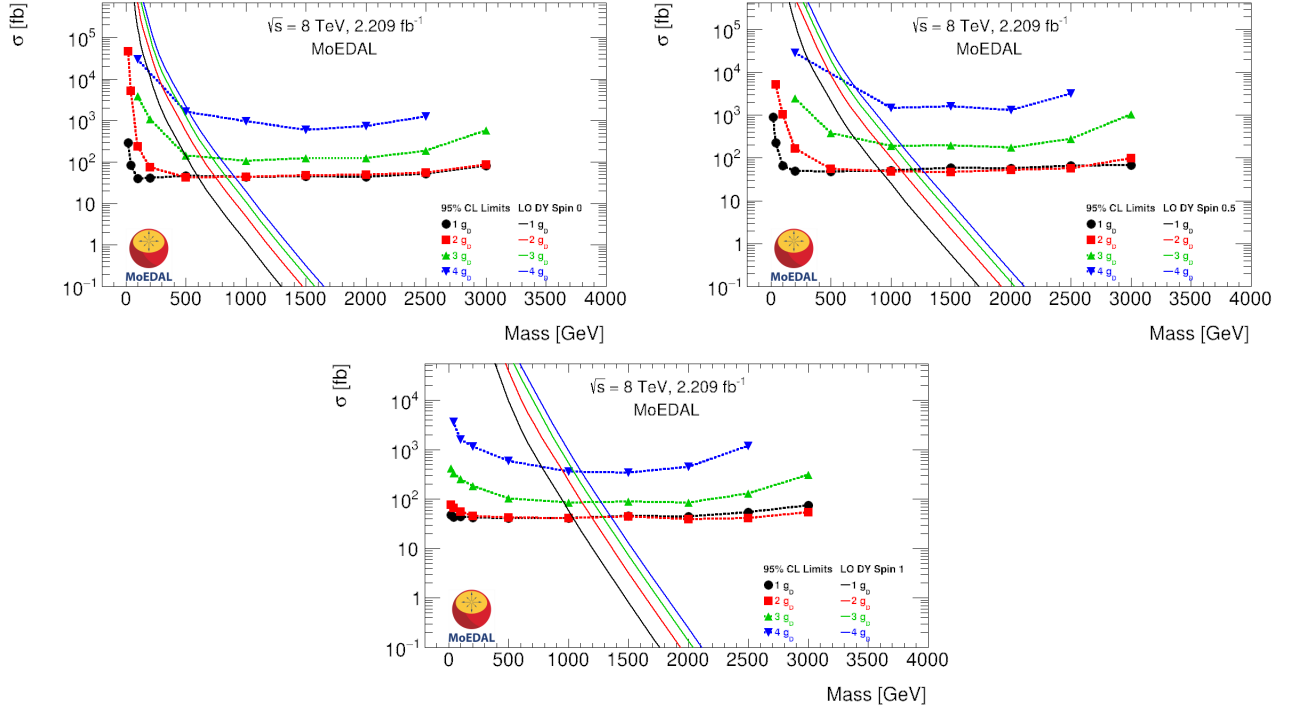


FIG. 15. 95% CL mass limits in a DY production model of spin-0, spin-1/2 and spin-1 monopole pair direct production in LHC  $pp$  collisions.

518 8.0 radiation lengths ( $X_0$ ) in thickness and on average  
 519 around 1.4  $X_0$  [42] thick. The main contribution to the  
 520 systematic uncertainty in this analysis arises from the esti-  
 521 mate of the material in the GEANT4 geometry descrip-  
 522 tion. The uncertainty in the material map is modelled  
 523 by two geometries which represent an excess and a deficit  
 524 of material, using conservative estimates of uncertainties  
 525 on material thicknesses and densities, compared to the  
 526 best assessment of the material budget that is compati-  
 527 ble with direct measurement and existing drawings.

528 This systematic uncertainty in the material map gives  
 529 rise to uncertainties in the DY acceptances. For singly  
 530 charge monopoles ( $|g| = g_D$ ) the resulting relative un-  
 531 certainty is of the order of 10% [8]. This uncertainty  
 532 increases with electric and magnetic charge. For a dou-  
 533 bly charged monopoles ( $|g| = 2g_D$ ) it is of the order of  
 534 10 - 20% for intermediate masses, around 1 TeV.

535 Other sources of systematic error are an uncertainty  
 536 due to a conservative estimate of 1 cm uncertainty in the  
 537 trapping detector position. Simulations show this error  
 538 lies in the range 1-17% [8]. Another source of systematics  
 539 is the uncertainty in  $dE/dx$  as a function of  $\beta$ , result-  
 540 ing in a 1-10% relative uncertainty in the acceptance [8].

541 In the case of monopoles and HECOS a systematic  
 542 error on the variable  $p$ , due to the NTD etching and  
 543 calibration process is given in Figure 10 (bottom). This  
 544 error on  $p$  can give rise to an error on the threshold value  
 545 for detection of the plastic as well as an error on the

546 variation of efficiency with angle of the NTD. However,  
 547 these uncertainties are negligible compared to the error  
 548 on the material map discussed above. All of the above  
 549 sources of systematic error were added in quadrature and  
 550 included in the final limit calculation.

551 We calculated the 95% C.L. upper limits to the  
 552 cross-section using as a measure a Drell–Yan model  
 553 for HECO and magnetic monopole production assum-  
 554 ing a  $\beta$ -independent monopole coupling and that the  
 555 monopole can have a spin of 0, 1/2 and 1. The limit  
 556 curves obtained are shown in Figure 14 for HECOs. For  
 557 monopoles the cross section upper limits versus mass are  
 558 given in Figure 15 for spin 0, 1/2 and 1. The values of the  
 559 95% C.L. mass limits are listed in Table II and Table III,  
 560 for HECOs and magnetic monopoles, respectively.

## 601 CONCLUSIONS

562 Both MoEDAL’s prototype NTD system and alu-  
 563 minium elements of the MoEDAL MMT detector, were  
 564 exposed to 8 TeV LHC collisions during LHC’s Run-1. At  
 565 the end of Run-1 both detector systems were examined  
 566 for the presence of magnetic monopoles and/or HECOs.  
 567 The NTDs were etched and scanned to reveal evidence  
 568 for the passage of a magnetic monopole or a HECO us-  
 569 ing semi-automatic and manual optical microscopes.  
 570 In the case of the MMT a SQUID-based magnetometer was

TABLE II. 95% CL mass limits for the HECO search corrected.

	Electric charge (e)														
	10	15	20	25	50	75	100	125	130	140	145	150	160	170	180
Spin	95% CL mass limits [GeV]														
0	30	110	220	270	560	560	540	500	500	470	470	450	400	-	-
1/2	100	270	420	550	770	760	700	600	590	560	550	-	-	-	-
1	-	360	550	700	1010	1020	1000	960	940	920	910	890	870	850	840

TABLE III. 95% CL mass limits for the magnetic monopole search.

	Magnetic charge ( $g_D$ )			
	1	2	3	4
Spin	95% CL mass limits [GeV]			
0	590	740	710	520
1/2	910	1090	1020	700
1	1030	1190	1190	1110

571 also utilized to search for the presence of trapped mag- 600  
572 netic charge. This is the first time that search results  
573 utilizing the the NTD detectors are presented.

574 In previous MoEDAL searches [8] only MoEDAL's 600  
575 MMT detectors were utilized. Consequently, the HIP 603  
576 search was limited to Magnetic Monopoles. In this search 604  
577 the use of the NTDs allows the highly ionizing signature 605  
578 of the HIP to be registered. This permits both magneti- 606  
579 cally charged and electrically charged HIPs (HECOs) to 607  
580 be detected. 608

581 No magnetic monopole candidates were found. Con- 600  
582 sequently, limits on the DY production of magnetic 602  
583 monopole pair with cross-section in the range of approx- 603  
584 imately 40 fb to 5 pb were set for magnetic charges up 604  
585 to  $4g_D$  and mass as high as 1.2 TeV. These limits are 605  
586 not competitive with recent Run-2 collider limits [11, 15] 606  
587 despite the use of the NTDs as well as the MMT sub- 607  
588 detectors. This is due to a combination of: the limited 608  
589 acceptance of MoEDAL's MMT and NTD Run-1 proto- 609  
590 type detectors compared to Run-2; the smaller Run-1 610  
591  $E_{CM}$  and DY cross-section at Run-1; and the smaller 611  
592 luminosity of Run-1 compared to Run-2. 612

593 No evidence was found for DY produced HECO pairs. 600  
594 Thus, limits were placed on the DY production of HECO 602  
595 pairs with cross-sections from around 30 fb to 70 pb, for 603  
596 electric charges in the range 10e to 180e and masses from 604  
597 590 GeV to 1 TeV. The limits on the DY production 605  
598 of HECO are the strongest to date, in terms of charge 606  
599 reach, at a collider experiment [15]. 607

## ACKNOWLEDGMENTS

601 We thank CERN for the LHC's successful Run-2 op-  
602 eration, as well as the support staff from our institu-  
603 tions without whom MoEDAL could not be operated.  
604 We acknowledge the invaluable assistance of particu-  
605 lar members of the LHCb Collaboration: G. Wilkin-  
606 son, R. Lindner, E. Thomas and G. Corti. Comput-  
607 ing support was provided by the GridPP Collabora-  
608 tion, in particular by the Queen Mary University of  
609 London and Liverpool grid sites. This work was sup-  
610 ported by grant PP00P2\_150583 of the Swiss NSF; by  
611 the UK Science and Technology Facilities Council, via the  
612 grants, ST/L000326/1, ST/L00044X/1, ST/N00101X/1  
613 and ST/P000258/1; by the Generalitat Valenciana via  
614 a special grant for MoEDAL and via the projects  
615 PROMETEO-II/2017/033 and PROMETEO/2019/087;  
616 by MCIU / AEI / FEDER, UE via the grants FPA2016-  
617 77177-C2-1-P, FPA2017-85985-P, FPA2017-84543-P and  
618 PGC2018-094856-B-I00; by the Physics Department of  
619 King's College London; by NSERC via a project grant;  
620 by the V-P Research of the University of Alberta (UofA);  
621 by the Provost of the UofA); by UEFISCDI (Romania);  
622 by the INFN (Italy); by the Estonian Research Council  
623 via a Mobilitas Plus grant MOBTT5; and by a National  
624 Science Foundation grant (US) to the University of Al-  
625 abama MoEDAL group.

---

626 \* Also at Int. Centre for Theoretical Physics, Trieste, Italy  
627 † CAPSS, Department of Physics Bose Institute, Kolkata,  
628 India

- <sup>‡</sup> Also at National Institute of Chemical Physics & Biophysics, Tallinn, Estonia  
<sup>§</sup> Also at Dept. of Physics, Faculty of Science, Beni-Suef University, Egypt  
<sup>¶</sup> Now deceased  
<sup>\*\*</sup> Also at Physics Department, University of Regina, Regina, Saskatchewan, Canada  
<sup>††</sup> Corresponding author: Laura.Patrizii@bo.infn.it  
<sup>‡‡</sup> Also at Research Centre for Astronomy, Astrophysics and Geophysics, Algiers, Algeria
- [1] M. Fairbairn et al., Stable Massive Particles at Colliders, Phys. Rept. 438 (2007).  
[2] L. Patrizii and M. Spurio, Status of Searches for Magnetic Monopoles, Annu. Rev. Nucl. Part. Sci. 65, 279 (2015)  
[3] B. Acharya et al., MoEDAL Collaboration, Physics Programme Of The MoEDAL Experiment At The LHC, Int. J. Mod. Phys. A29, 1430050 (2014).  
[4] G. Aad et al., ATLAS Collaboration, Search for massive long-lived highly ionizing particles with the ATLAS detector at the LHC, Phys. Lett. B 698, 53 (2011).  
[5] G. Aad et al., ATLAS Collaboration, Search for Magnetic Monopoles in  $\sqrt{s} = 7$  TeV pp Collisions with the ATLAS Detector, Phys. Rev. Lett. 109, 261803 (2012),  
[6] G. Aad et al., ATLAS Collaboration, Search for long-lived, multi-charged particles in pp collisions at  $\sqrt{s} = 7$  TeV using the ATLAS detector, Phys. Lett. B 722, 305 (2013).  
[7] G. Aad et al, ATLAS Collaboration, Search for magnetic monopoles and stable particles with high electric charges in 8 TeV pp collisions with the ATLAS detector, Phys. Rev. D 93, 052009 (2016).  
[8] B. Acharya et al., MoEDAL Collaboration, Search for magnetic monopoles with the MoEDAL prototype trapping detector in 8 TeV proton-proton collisions at the LHC, JHEP 08, 067 (2016).  
[9] B. Acharya et al., MoEDAL Collaboration, Search for magnetic monopoles with the MoEDAL forward trapping detector in 13 TeV proton-proton collisions at the LHC, Phys. Rev. Lett. 118, 061801 (2017).  
[10] B. Acharya et al., MoEDAL Collaboration, Search for magnetic monopoles with the MoEDAL forward trapping detector in 2.11 fb<sup>-1</sup> of 13 TeV proton-proton collisions at the LHC, Phys. Lett. B 782, 510 (2018).  
[11] B. Acharya et al., MoEDAL Collaboration, Magnetic Monopole Search with the Full MoEDAL Trapping Detector in 13 TeV pp Collisions Interpreted in Photon-Fusion and Drell-Yan Production, Phys.Rev.Lett. 123, 021802 (2019).  
[12] ATLAS Collaboration, Search for heavy long-lived multi-charged particles in pp collisions at  $\sqrt{s} = 8$  TeV using the ATLAS detector, Eur. Phys. J. C 75, 362 (2015).  
[13] S. Chatrchyan et al., CMS Collaboration, Searches for long-lived charged particles in pp collisions at  $\sqrt{s} = 7$  and 8 TeV, JHEP 07, 122 (2013) 122.  
[14] M. Aaboud, ATLAS Collaboration, Search for heavy long-lived multi-charged particles in proton-proton collisions at  $\sqrt{s} = 13$  TeV using the ATLAS detector, Phys. Rev. D 99, 052003 (2018) 052003.  
[15] G. Aad et al., The ATLAS Collaboration, Search for Magnetic Monopoles and Stable High-Electric Charged Objects in 13 TeV Proton-Proton Collisions with the ATLAS Detector, Phys. Rev. Lett., 124, 3 031802 (2020).  
[16] S. Burdin et al., Non-collider searches for stable massive particles, Phys. Rept. 582, 1(2015).  
[17] L. Patrizii, Z. Sahnoun, and V. Togo, Searches for cosmic magnetic monopoles: past, present and future, Phil. Trans. R. Soc. A 377: 20180328 (2019).  
[18] J. Beringer et al. (Particle Data Group), Phys. Rev. D86, 0100001 (2012).  
[19] P. A. M. Dirac, Quantised Singularities in the Electromagnetic Field, Proc. Roy. Soc. A 133, 60 (1931).  
[20] G. 't Hooft, Magnetic Monopoles in Unified Gauge Theories, Nucl. Phys. B79, 276 (1974).  
[21] A. M. Polyakov, Particle Spectrum in the Quantum Field Theory, JETP Lett. 20, 194 (1974).  
[22] H. Georgi and S. Glashow, Unified weak and electromagnetic interactions without neutral currents. Phys. Rev. Lett, 28, 1494 (1972).  
[23] H. Georgi and S. Glashow, S. Unity of all elementary particle forces. Phys. Rev. Lett, 32, 438–441 (1974).  
[24] Y.M. Cho and D. Maison, Phys. Lett. B391, 360 (1997).  
[25] W.S. Bae and Y.M. Cho, JKPS46, 791 (2005).  
[26] Y. M. Cho, K. Kim and J. H. Yoon, Eur. Phys. J. C75, no. 2, 67 (2015).  
[27] J. Schwinger, A Magnetic Model of Matter. Science. 165, 757-761 (3895).  
[28] J. Ellis, N. E. Mavromatos, T. You, The Price of an Electroweak Monopole, Phys. Lett. B756, 20-35 (2016).  
[29] B. Holdom, J. Ren, and C. Zhang, Quark Matter May Not Be Strange, Phys. Rev. Lett. 120, 222001 (2018).  
[30] E. Farhi and R. Jaffe, Strange matter, Phys. Rev. D30, 2379 (1984).  
[31] S. Coleman, Q-balls, Nucl. Phys. B262, 263 (1985).  
[32] A. Kusenko and M. E. Shaposhnikov, Supersymmetric Q-balls as dark matter, Phys. Lett. B418(1998) 46.  
[33] B. Koch, M. Bleicher, and H. Stöcker, Black holes at LHC? J. Phys. G34 S535 (2007).  
[34] E. V Benton and W. D. Nix, The restricted energy loss criterion for registration of charged particles in plastics, NIM 67, 343-347 (1969).  
[35] L.P. Gamberg, G.R. Kalbfleisch and K.A. Milton, Direct and indirect searches for low mass magnetic monopoles, Found. Phys. 30, 543 (2000) 543; Private communication from Kimball A. Milton, January 26th 2021.  
[36] C.J. Goebel, Binding of nuclei to monopoles, in Monopole '83, J.L. Stone ed., Plenum(1984), p. 333.  
[37] L. Bracci and G. Fiorentini, Interactions of Magnetic Monopoles With Nuclei and Atoms, Nucl. Phys. B 232, 236 (1984).  
[38] K. Olausen and R. Sollie, Form-factor effects on nucleus-magnetic monopole binding, Nucl.Phys.B 255, 465 (1985).  
[39] A. De Roeck et al., Development of a magnetometer-based search strategy for stopped monopoles at the Large Hadron Collider, Eur. Phys. J. C72,2212 (2012).  
[40] S. Balestra et al., Magnetic monopole search at high altitude with the SLIM experiment, Eur. Phys. J. C 55, 57–63 (2008).  
[41] S. Balestra et al., Bulk etch rate measurements and calibrations of plastic nuclear track detectors, NIM-B 254, 254-258 (2007).  
[42] A. A. Alves Jr., et al., LHCb Collaboration, The LHCb Detector at the LHC, JINST 3, S08005 (2008).  
[43] L.A. Harland-Lang, V.A. Khoze, M.G. Ryskin “Exclusive LHC physics with heavy ions: SuperChic 3” arXiv:1810.06567  
[44] P.J.W.Faulkner et al., GridPP: development of the UK computing Grid for particle physics, Journal of Physics

- <sup>757</sup> G: Nuclear and Particle Physics, 32(1), N1-N20 (2006)
- <sup>758</sup> [45] D. Britton et al., GridPP: The UK grid for particle <sup>760</sup> [46] M. Ambrosio et al., MACRO Collaboration, Eur. Phys.
- <sup>759</sup> physics, Phil. Trans. R. Soc. 367(1897):2447-57 (2009) <sup>761</sup> J. C25 511 (2002).
- <sup>762</sup> [47] S. Balestra et al., The SLIM Collaboration, Magnetic
- <sup>763</sup> Monopole Search at high altitude with the SLIM exper-
- <sup>764</sup> iment, Eur. Phys. J.C 55, 57-63 (2008).